Volume 12, Number 3, 2019. pp. 223-236

Jordan Journal of Physics

ARTICLE

The Collision-Induced Absorption Spectra of Hydrogen Complexes in the Second Overtone Band

M. Abu-Kharma[a], **Mahmoud H. Saleh**[a], **Z. M. Elimat**[b] and **W. J. Kadhem**[b]

[a] *Department of Physics, Faculty of Science, Al-Balqa Applied University, Al-Salt 19117, Jordan.*

[b] *Department of Physics and Basic Sciences, Faculty of Engineering Technology, Al-Balqa Applied University, Amman 11134, Jordan..*

Received on: 03/02/2019; Accepted on: 16/4/2019

Abstract: The second overtone band (3-0) of pure hydrogen spectra at different temperatures and hydrogen gas densities is reviewed with particular emphasis on the most recent theoretical and experimental results. Different experimental and theoretical techniques were used to record and calculate the second overtone band profiles. The calculated theoretical binary and ternary absorption coefficients are in good agreement with experimental values obtained. Different line shapes were used to fit the experimental profiles. The fitting values are tabulated in the references therein. The goal of this article is to draw the attention of the absorption spectroscopy community to the fact that there have been only a few investigations on the latter subject on the second overtone band (3-0) on hydrogen, even though the investigations on the other bands are quite abundant.

Keywords: Collision-induced spectroscopy, Infrared absorption, CIA, IR spectra, H_2, Second overtone band, Line shape functions, Roto-vibrational state.

PACS: 33.15.Mt, 33.20.a, E33.20.Vq

Introduction

There has been substantial interest in the study of the hydrogen spectra driven by the fact that the hydrogen molecule is the simplest of all diatomic molecules. Further, hydrogen is the most abundant element in the atmospheres of the planets and stellar objects and constitutes about 75% of all matter in the universe. Indeed, the collision mechanism of H_2-H_2 yields the associated thermal emission and absorption spectra. Within this context, the second overtone band of hydrogen is important for studies of both planetary and stellar atmospheres [1-8] and appears between the visible and the near-infrared spectral region, approximately between 11000 and 13800 cm^{-1}. The properties of this band have not been precisely delineated due to the weakness of absorption and the experimental difficulties encountered in its investigation. It consists of the short-range electron-overlap interaction and the long-range quadrupole induced transitions of the types:

(a) single transitions ($3 \leftarrow 0$) $Q_3(J) + Q_0(J)$, $S_3(J) + Q_0(J)$ and $Q_3(J) + S_0(J)$,

(b) double transitions [($2 \leftarrow 0$) + ($1 \leftarrow 0$)] $Q_2(J) + Q_1(J)$, $S_2(J) + Q_1(J)$, $Q_2(J) + S_1(J)$ and $S_2(J) + S_1(J)$, and

(c) triple transitions [($1 \leftarrow 0$) + ($1 \leftarrow 0$) + ($1 \leftarrow 0$)] $Q_1(J) + Q_1(J) + Q_1(J)$,

where the subscripts 0,1,2 and 3 indicate Δ v, the change in the vibrational quantum number and J indicates the rotational quantum number.

The collision-induced absorption spectrum (CIA) arises from transient electric dipole moments that exist during binary, ternary and

Corresponding Author: M. Abu-Kharma **Email**: mkharma@bau.edu.jo

higher-order collisions. Three mechanisms contribute to the induction of an electric dipole moment: (a) the polarization of one hydrogen molecule in the multipolar field of another hydrogen molecule, (b) electron exchange in the H_2-H_2 molecule at near range and (c) the dispersion interaction. When the transient induced-dipole moments interact with the electromagnetic field from an infrared radiation source, the colliding molecules absorb infrared radiation in the spectral regions corresponding to roto-vibrational, pure rotational and translational states. The major properties of the absorption lines in this case are: (a) the line widths are large, typically 10-50 cm^{-1}; (b) the absorption profiles and the integrated absorption coefficients $\int \alpha(v)\, dv$ are proportional to the square and the cube of the density for pure gases in the case of binary and ternary collisions, respectively; (c) the integrated intensity of the band is temperature-dependent and (d) a dip at $Q_3(1)$ with characteristic low and high wavenumber components Q_P and Q_R is observed which is temperature-dependent.

There have been many theoretical and experimental investigations on the CIA of the second overtone band of hydrogen at different temperatures [1-20]. Initially, Herzberg identified a diffuse feature at 12093 cm^{-1}, observed in the spectra of Uranus and Neptune by Kuiper earlier, as the collision-induced $S_3(0)$ line of the second overtone band of H_2 [2].

Later, Herzberg photographed the second overtone band of H_2 at a gas pressure of 100 atm at 78K with a path length of 80 m. Herzberg interpreted the spectrum as consisting of a pure second overtone band, in which one of the two colliding molecules makes a vibrational transition $\Delta v = 3$ such as: $Q_3(J) + Q_0(J)$ and a double vibrational band in which one molecule makes a vibrational transition $\Delta v = 2$, while the second molecule makes a vibrational transition $\Delta v = 1$, such as: $Q_1(J) + Q_2(J)$, $Q_1(J) + S_2(J)$ and $Q_2(J) + S_1(J)$ [3]. Subsequently, Hunt recorded the same band at room temperature and pressures up to 2200 atm [4].

A few years later, Mckellar and Welsh recorded the second overtone band spectra of H_2 at gas densities of about 37 amagat (1amagat = 44.614981 mol/m^3) at 85 K with a path length of 137m. Their analysis of the absorption profiles showed several discrepancies between the experimental and calculated profiles. They suggested that these discrepancies arise because of the overlap-induction contribution to the 3-0 band that has not been included in their calculations [5, 6].

Further down the road, Gillard recorded the induced spectra of H_2 and D_2 in the second overtone region at 77K and densities in the range 500-930 amagat using a 2m absorption cell. He was the first to record the second overtone band of deuterium. Further, he also interpreted the observed peaks in the spectra and calculated the binary and ternary absorption coefficients of the measured integrated absorption. But, he met some difficulties in the analysis of the CIA spectra due to lack of information on the available values of the quadrupole-moment matrix elements, polarizability and anisotropy of the polarizability of H_2 and D_2 [7].

Fan Xiang recorded the absorption spectra of the second overtone region of H_2 for gas densities up to 1000 amagat at 77, 201 and 298 K using a 2m absorption cell. He observed a dip at $Q_3(1)$ with characteristic low and high wavenumber components Q_P and Q_R. The dip occurs due to the short-range electron-overlap interaction of the collisions of the second overtone band. Good agreement between the experimental and calculated absorption profiles has been obtained by reducing the matrix elements of the quadrupolar moment <0J|Q|v'J'> for the first and second overtone band by a factor of 0.68 [8]. Reddy et al. [9] presented the first observation of simultaneous vibrational transitions involving three molecules in CIA spectra. They analyzed the experimental profiles resulting from triple-collision transitions using the Lorentz line-shape function as well as Birnbaum-Cohen line-shape function.

Brodbeck et al. recorded the CIA spectra of H_2 in the region of the second overtone at 0.8μm and temperatures of 298 and 77.5 K for gas densities ranging from 100 to 800 amagats. The spectra were recorded with a Fourier transform spectrometer using two high-pressure absorption cells. These authors obtained the binary absorption coefficients by extrapolating their measurements and compared the calculated binary absorption coefficients with results from *ab initio* calculations [11, 12]. More recently, Abu-Kharma [18-20] studied the second overtone bands of hydrogen and deuterium at different temperatures for gas densities up to 1000 amagat. Also, the binary and ternary absorption coefficients have been determined. Satisfactory agreement between the calculated and the recorded profiles has been observed.

Many methods have been used to calculate the spectral lines of the second overtone band [7-19]. In parallel to experimental research, theoretical investigations took place, such as those following. Yi Fu et al. conducted a quantum mechanical computation of the collision-induced roto-vibrational absorption spectra of hydrogen in the second overtone band [13]. Borysow et al. presented a semi-empirical numerical method to compute the binary collision-induced roto-vibrational absorption spectra of hydrogen molecules in the second overtone band of hydrogen, at temperatures from 50 to 500 K [14]. They compared their semi-empirical model with the CIA spectra of normal hydrogen for the second overtone band at 77.5 K and 298 K measured by Brodbeck et al. [15]. Brodbeck et al. studied the CIA spectra in the second overtone region at ambient and liquid nitrogen temperatures. They found good agreement between the experimental and calculated binary absorption coefficients [11, 12]. Abel studied the CIA in the roto-translational band of H_2-H_2 and in the fundamental, first and second overtone bands of H_2 in dense hydrogen gas. He compared the existing measurements of the latter overtones of H_2 with *ab initio* calculations based on new dipole and potential energy surfaces. Over the full range of frequencies considered, the agreement between theoretical calculations and measurements is remarkable. His method can reproduce the measured spectra with high accuracy [16]. Abel et al. [17] computed the binary absorption coefficients at wavelengths near 5 µm at temperatures of 77.5 and 297K based on an *ab initio* interaction-induced dipole surface of collisionally interacting molecular hydrogen pairs H_2-H_2 and compared their results with an existing laboratory measurement.

Moraldi and Frommhold [10] studied the triple transition $Q_1(J_1) + Q_1(J_2) + Q_1(J_3)$ near 12466 cm^{-1} in compressed hydrogen. They used the model of the overlap-induced, irreducible, ternary dipole component of three interacting H_2 molecules to calculate the intensity of the triple Q_1 transition observed by Reddy et al. [9] in pure hydrogen gas near 12466 cm^{-1}. The calculated intensities agree with measurements within a factor of 2 or 3.

In the present paper, we present the collision-induced absorption spectra of H_2-H_2 with emphasis on the second overtone band. Also, we include the most recent experimental and theoretical results.

Experimental and Theoretical Details

The pressure cells used in the CIA experiments are constructed of polished stainless steel and equipped with sapphire windows. The lengths of the cells are 300.5 cm, 215.25 cm [11, 12], 194.2 cm, 194.5cm, 194.8cm [7,8]. Further, an absorption optical path of 80m or 137m length has been obtained with a cell 3.5 m long [5].

The spectra are recorded using different spectrometers:

1- A Perkin-Elmer model 112G single beam double pass grating spectrometer equipped with a plane grating of 300 lines/mm. The spectral resolution is ~2cm^{-1} at 11782 cm^{-1}.

2- A Bruker IFS 66V FT spectrometer with a resolution of 0.5 cm^{-1}.

The infrared source of radiation is a General Electric FFJ 600 W quartz line projection lamp housed in a water-cooled brass jacket.

Different detectors suitable and sensitive to the second band region have been used:

1- A Hammamatsu model R758 photomultipliers tube.

2- A Si diode running at room temperature.

For more experimental details, the reader is referred to the references therein.

Binary and Ternary Absorption Coefficients

The absorption coefficient α(ν) of a pure gas at a given wavenumber ν is:

$$\alpha(v) = \frac{1}{l}\ln\left[\frac{I_0(v)}{I(v)}\right] \tag{1}$$

where I_0 (v) is the transmitted intensity of the radiation source through an evacuated cell of optical path length l and I (v) is the transmitted intensity through the cell which contains the absorbing pure gas at a given density ρ (amagat). The dimensionless absorption coefficient reads:

$$\tilde{\alpha}(v) \equiv \frac{\alpha(v)}{v} \tag{2}$$

which is given by:

$$\tilde{\alpha}(v) = \sum_{m\,n} \frac{\tilde{\alpha}^0_{nm} W_n(\Delta v)}{1+e^{(-hc\Delta v/kT)}} \tag{3}$$

where *n* stands for the induction mechanism and *n = ov, q* or *h* are overlap, quadrupolar or hexadecapolar induction, respectively, *m* represents a specific transition arising from a given mechanism, $\widetilde{\alpha}_{nm}^{0}$ is a parameter equal to twice the maximum absorption coefficient at the frequency v_m and $W_n(\Delta v)$ with $\Delta v = v - v_m$ represents the line shape function of the *n* type. The factor $\left[1 + e^{(-hc\Delta v/kT)}\right]$ satisfies the detailed balance condition and converts the symmetric into asymmetric line shape function.

The integrated absorption coefficient for the pure gas is given by:

$$\int \alpha(v)dv = \alpha_1\rho^2 + \alpha_2\rho^3 + \cdots \qquad (4)$$

where $\alpha_1$and α_2 are the binary and ternary absorption coefficients. Eq. (4) can be rewritten in the form:

$$(1/\rho^2)\int \alpha(v)dv = \alpha_1 + \alpha_2\rho + \cdots \qquad (5)$$

The plot of $(1/\rho^2)\int \alpha(v)dv$ *versus* ρ gives a straight line of slope α_2 and an interception of α_1. The integrated binary absorption coefficient due to quadrupole induction for a given band is given by Poll [21]:

$$\tilde{\alpha}_{qm} = \frac{1}{\rho^2}\int \frac{\alpha_m(v)}{v}dv = \frac{4e^2\pi^2}{3\hbar c} n_0^2\, a_0^5 \left(\frac{a_0}{\sigma}\right)^5 \tilde{J}_2 X_{2m} \qquad (6)$$

where

$$X_{2m} = \sum P_{j1}P_{j2}\begin{bmatrix} C(J_1 2J_1'; 00)^2 \langle V_1\, J_1|Q_{21}|V_1'\, J_1'\rangle^2 \\ C(J_2 0J_2'; 00)^2 \langle V_2\, J_2|\alpha_2|V_2'\, J_2'\rangle^2 \\ \\ +C(J_2 2J_2'; 00)^2 \langle V_2\, J_2|Q_{21}|V_2'\, J_2'\rangle^2 \\ C(J_1 0J_1'; 00)^2 \langle V_1\, J_1|\alpha_1|V_1'\, J_1'\rangle^2 \end{bmatrix} + Y_{2m} \qquad (7)$$

and

$$\tilde{J}_2 = 12\pi \int_0^\infty x^{-6}\, g_0\,(x)\mathrm{d}x. \qquad (8)$$

where *e* is the charge of an electron, $n_0 = 2.387\times10^{19}$ molecules/cm^3 is Loschmidt's number, a_0 is the Bohr radius and σ is the intermolecular separation corresponding to the intermolecular potential V(σ) = 0, $\langle vj|Q_2|v'j'\rangle$ is the matrix element for the quadrupole induction, $\langle vj|\alpha|v'j'\rangle$ is the matrix element of the isotropic polarizability, $g_0\,(x)$ is the pair correlation function for the gas, $x = R/\sigma$, R being the intermolecular separation and the numbers 1 and 2 refer to the two colliding molecules. P_J stands for the normalized Boltzmann factors:

$$P_J = \frac{g_T(2J+1)e^{\left(-E_J/kT\right)}}{\sum_J g_T(2J+1)e^{\left(-E_J/kT\right)}} \qquad (9)$$

with g_T being the nuclear statistical weight of the molecule in each rotational state, E_J is the rotational energy and g_T is 1 and 3 for the even and odd *J*, respectively, for H$_2$. *C(JLJ';00)*'s are Clebsch-Gordan coefficients, the values of which are given by Rose [25]. The Y_{2m} term is small compared to X_{2m} and accounts for the contribution of the anisotropy of polarizability of the quadrupole transitions.

The Line Shape Function

The line shape function in Eq. (3), $W_n(\Delta v)$ for the overlap transition is represented by:

$$W_{ov}\,(\Delta v) = \left[\left(\frac{2\Delta v}{\delta_d}\right)^2 K_2\left(\frac{2\Delta v}{\delta_d}\right)\right]\left[1 - \gamma\left\{1 + \left(\frac{\Delta v}{\delta_c}\right)^2\right\}^{-1}\right] \qquad (10)$$

It is formed of two parts: the intra-collisional line shape function (Levine-Birnbaum shape function) and the inter-collisional line shape function [26], where K_2 is the modified Bessel function of the second kind, δ_d is the intra-collisional half-width at half-height, γ is a constant that equals one unit yields zero absorption at the dip at v_m and δ_c is the inter-collisional half-width at half -height equal to $(1/2\pi\, c\tau_c)$, where τ_c is the mean time between collisions.

The line shape function for the quadrupolar transitions is given by:

(a) the dispersion-type function:

$$W_q(\Delta v) = \frac{1}{1+\left(\frac{\Delta v}{\delta_q}\right)^2} \qquad (11)$$

where δ_q is the quadrupolar half-width at half-height. Gillard [7] modeled quadrupolar transitions with a modified dispersion line-shape function:

$$W_q(\Delta v) = \frac{1}{1+\left(\frac{\Delta v}{\delta_{q1}}\right)^2+\left(\frac{\Delta v}{\delta_{q2}}\right)^4} \qquad (12)$$

where the fourth-power term better reproduces the spectrum.

(b) The Birnbaum-Cohen (BC) line shape function is given by:

$$W_q^{BC}(\Delta v) = \frac{1}{2\pi^2 c\delta_1}\exp\left(\frac{\delta_1}{\delta_2}\right)\exp\left(\frac{hc\Delta v}{2kT}\right)\frac{zK_1(z)}{1+(\Delta v/\ _1)} \quad (13)$$

where

$$z = [1+(\Delta v\delta_1)^2]^{1/2}\left[\left(\frac{\delta_1}{\delta_2}\right)^2+\left(\frac{hc\delta_1}{2\pi kT}\right)^2\right]^{1/2} \quad (14)$$

$\Delta v = v - v_m$, $K_1(z)$ is a modified Bessel function of the second kind of order 1, $\delta_i = 1/2\pi c\tau_i$ is a wavenumber parameter and τ_i is a characteristic time in the dipole moment correlation function. Lewis [22] modified the BC line-shape with a new one referred to as the Lewis-Birnbaum-Cohen (LBC) line-shape which is given by:

$$W^{LBC}(\Delta\omega) = \frac{2}{1+e^{-\beta\hbar\Delta\omega}}\frac{e^{\tau_2/\tau_1}}{\pi}\frac{\tau_2}{\sqrt{1+\Delta\omega^2\tau_1^2}}K_1\left(\sqrt{1+\Delta\omega^2\tau_1^2}\,\frac{\tau_2}{\tau_1}\right) \quad (15)$$

where $\Delta\omega = \omega - \omega_m + \omega_s$, with ω_m being the frequency of the m^{th} transition ($\omega = c/v$). The LBC line-shape function is derived from the BC line-shape function with a slight modification of the procedure used. Beside the semi-line-shapes discussed earlier, there are:

(a) A semi-empirical numerical method to calculate the binary collision-induced roto-vibrational absorption spectra of H_2-H_2 complexes in the second overtone region of hydrogen at temperatures from 50-500 K. The numerical procedure uses simple analytical model line-shapes and can generate the roto-vibrational CIA spectra of hydrogen pairs easily [14].

(b) Quantum line-shape functions which are derived from quantum mechanical computations of the roto-vibrational CIA spectra of H_2-H_2 in the second overtone band [13].

Results and Discussion

Summary of Experimental Work

Illustrative examples of CIA spectra of the H_2-H_2 second overtone band in the pure gas at 77, 86, 201 and 298 K are shown in Figs. (1-4). Fig. 5 represents absorption profiles of the second overtone band of gaseous H_2-H_2 at 77, 201 and 298K obtained with a two-meter cell. Also, typical absorption profiles of deuterium in the pure gas at 77K and densities 685, 830 and 929 amagat in the second overtone region are shown in Fig. 6 by a plot of Log [$I_0(v)/I(v)$] *versus* the wave number ν(cm^{-1}). The recorded profiles mainly consist of the overlap component which occurs due to the short-range electron-overlap interaction of the collisions and the long-range quadrupole-induced transitions of the single, double and triple transitions. The possible quadrupolar and overlap transitions which contribute significantly to the absorption at different temperatures are listed in Table 1. These transitions are calculated from the constants of the free hydrogen molecules (Foltz et al. for *v=3* and Bragg et al. for *v=0,1* and *2* [23,24]).

Several features of these profiles are worth mentioning. First, the appearance of a characteristic dip in the $Q_3(J)$ lines with its low and high wave-number maxima Q_P and Q_R. The separation between Q_P and Q_R increases with density and becomes more obvious at room temperature. Further, the dip position is shifted to high wave-numbers with increasing density. The sharp absorption dip occurs due to the inter-collisional interference effect which arises from the negative correlations existing between the short-range overlap of dipole moments induced in successive collisions [26]. It appears that either the overlap induction is active in the 1-0, 3-0, 5-0, … etc. bands and absent in the 2-0, 4-0, 6-0, … etc. bands; or it is absent for some reason only in the first overtone band [5]. In the future, we shall seek to find an explanation for the latter absence. The line width increases with temperature. Second, the spectral band profiles defined by [$1/l\rho^2$] Ln(I_0)/(I) vary significantly with the gas density ρ [12]. The increase of α(ν) with the density, observed in the region 12400-12600 cm^{-1}, may be partially arising from the contribution of the ternary transitions. Third, the quadrupolar lines in the second overtone profiles appear to be somewhat narrower than the corresponding lines in the fundamental and first overtone bands. This is attributed to the diffusional narrowing which occurs at high densities used to record the second overtone region. Fourth, the recorded profile at 86 K shows no dip in the $Q_3(J)$ branch and only five peaks are displayed because of the low gas density used. Fifth, the number of peaks increases with decreasing temperature, as shown in Figs. 1 to 4. Absorption peak positions and the assignments of the transitions contributing to these peaks are listed in Table 2. The observed positions of the peaks 1 to 9 and their assignments are listed in Tables 1 and 2.

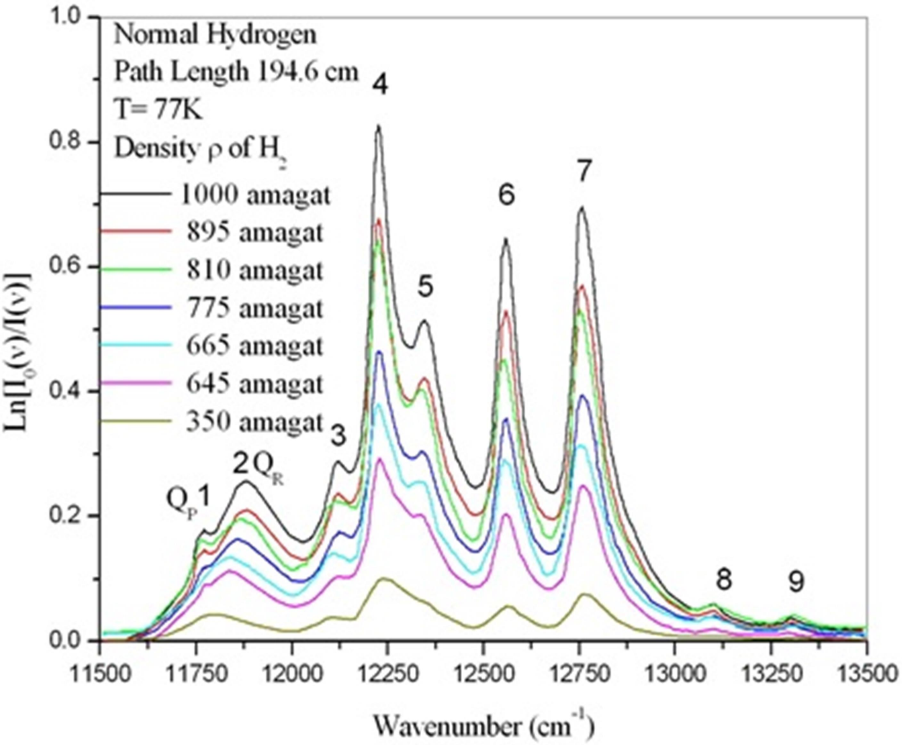

FIG. 1. Absorption profiles of the second overtone band of H_2 at 77 K with a path length of 194.2 cm.

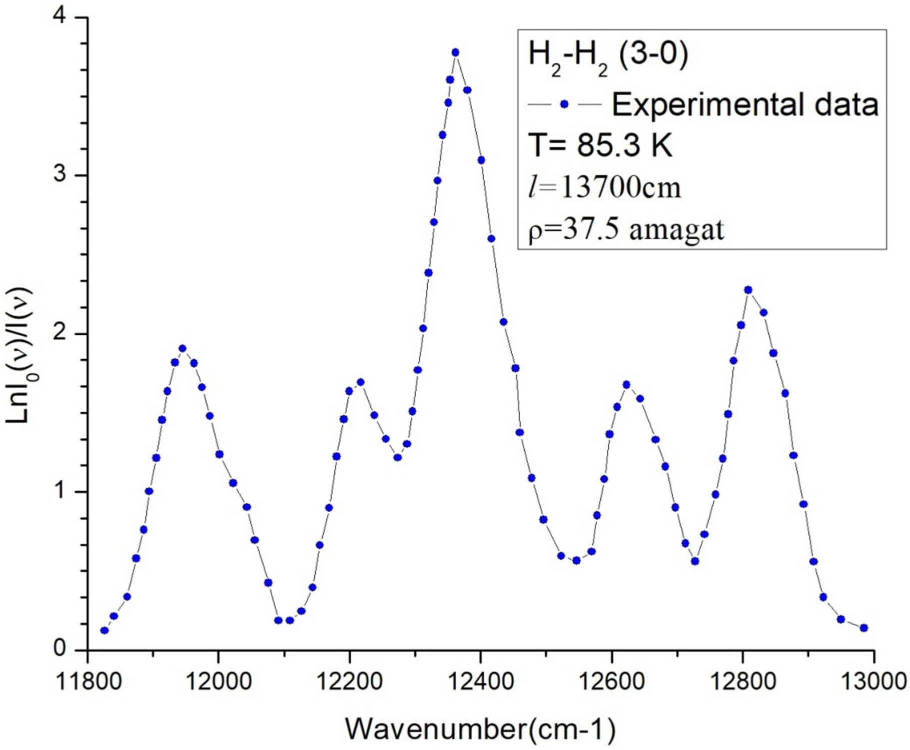

FIG. 2. Absorption profile of the second overtone band of normal hydrogen at 86 K with a path length of 137m [5].

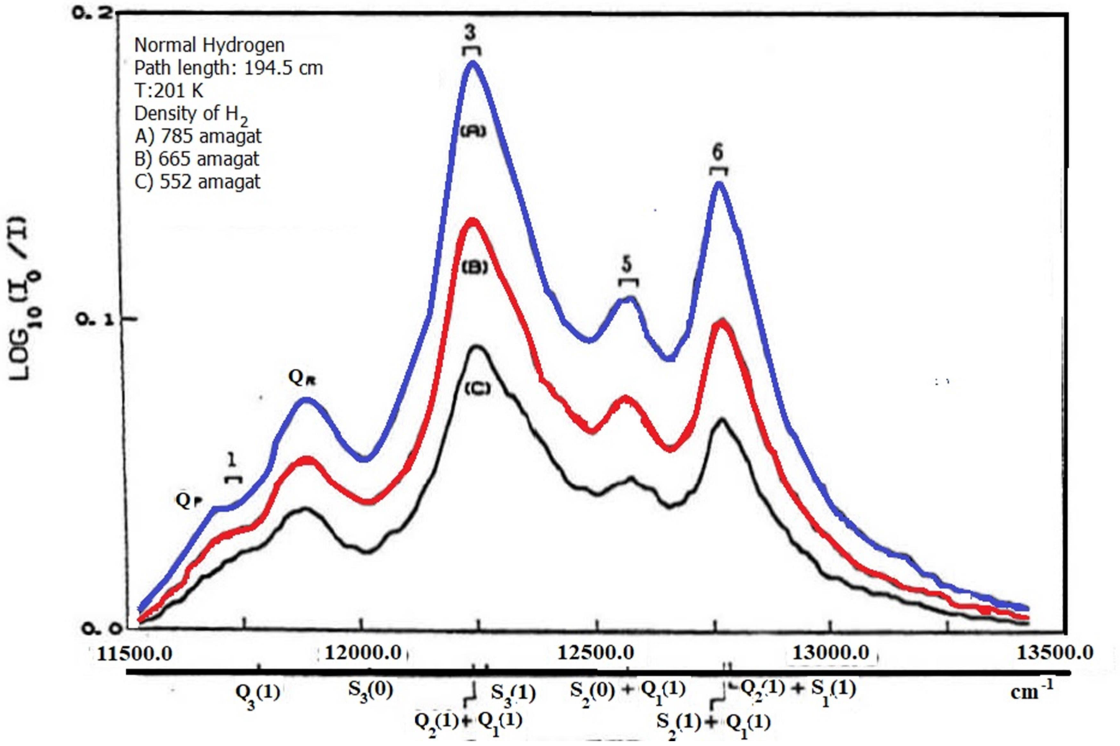

FIG. 3. Absorption profiles of the second overtone band of H_2 at 201 K with a path length of 194.5 cm.

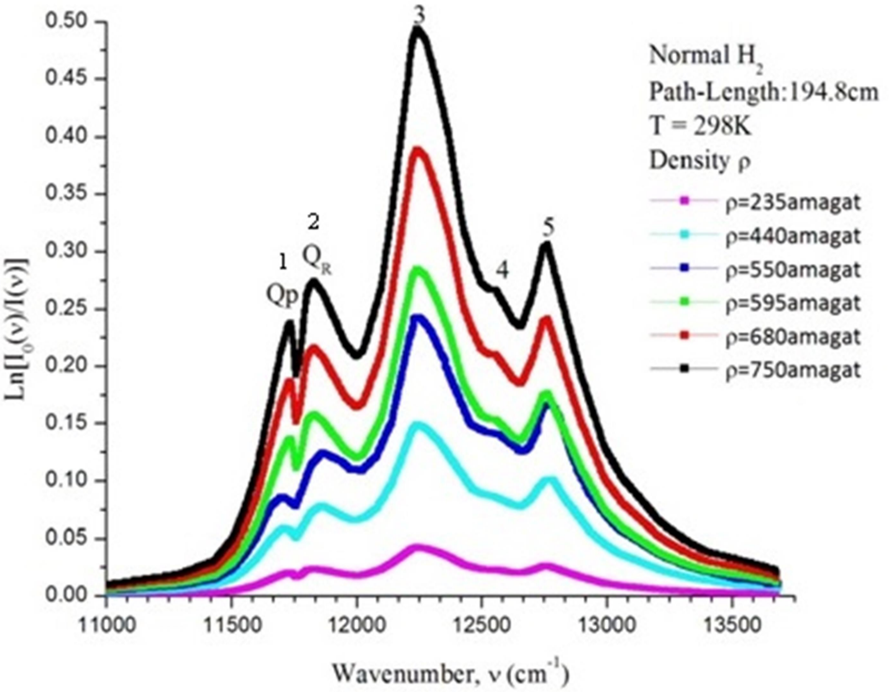

FIG. 4. Absorption profiles of the second overtone band of H_2 at 298 K with a path length of 194.8 cm.

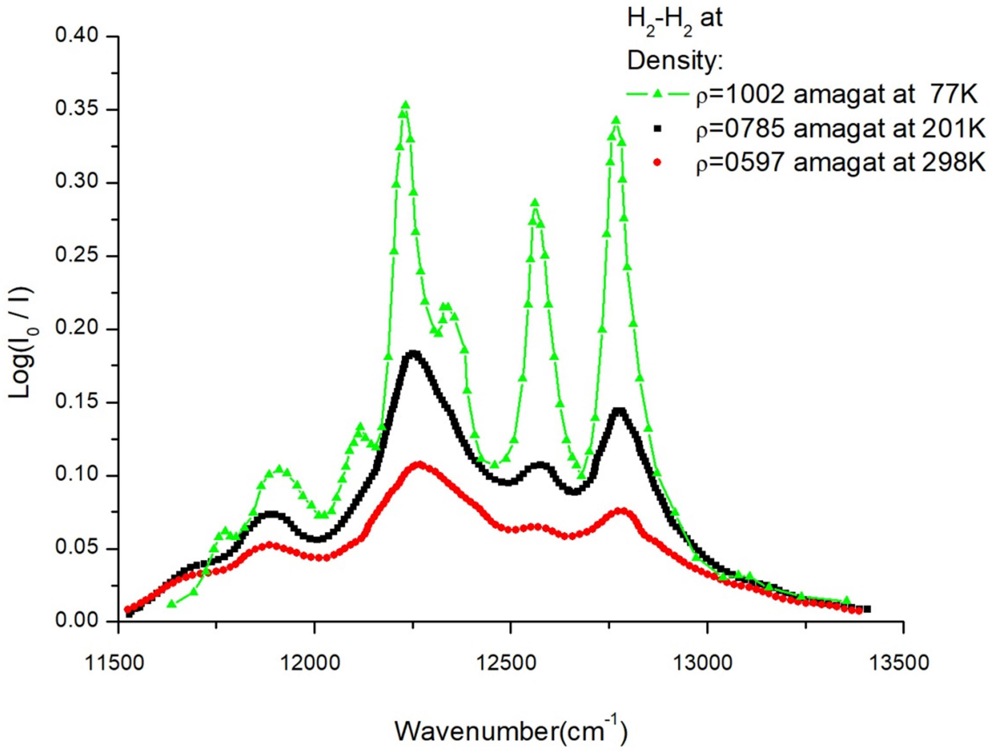

FIG. 5. Absorption profiles of the second overtone band of H_2 at 77, 201 and 298 K.

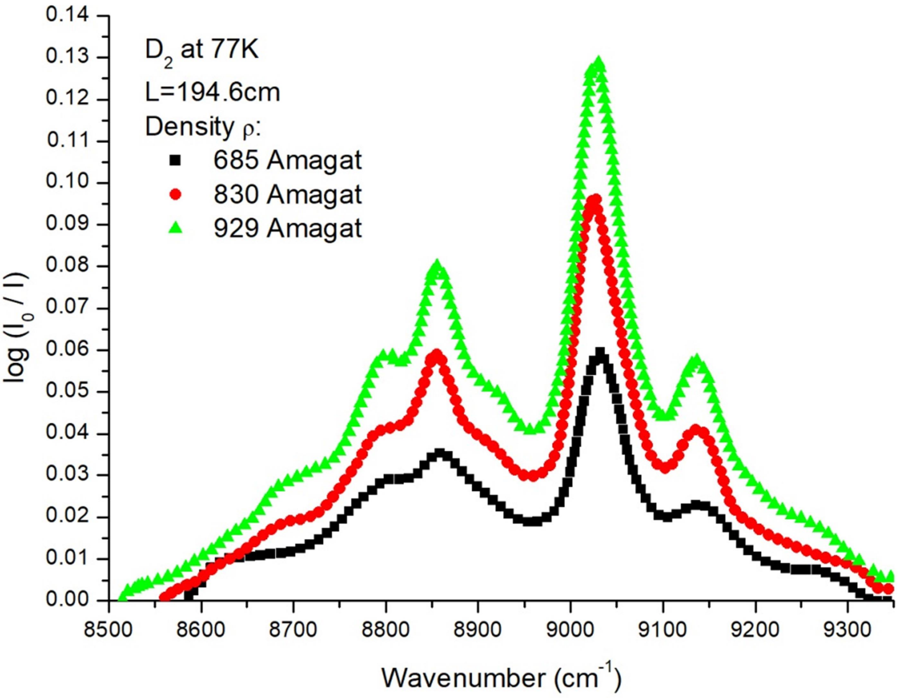

FIG. 6. Absorption profiles of the D_2 second overtone region at 77K with a path length of 194.6cm.

TABLE 1. Transitions that contribute to the (3-0) band of H_2-H_2 at different temperatures.

#	Transitions	Wavenumber (cm^{-1})	Number of components for different temperatures
1 Single Transitions	Q_3(J=0-5) + S_0(J=0-5)	11532-12997	4-22
	Q_3(J=0-5) + Q_0(J=0-5)	11550-11678	4-24
	S_3(J=0-3) + Q_0(J=0-5)	12085-12754	4-24
	S_3(J=0-3) + S_0(J=0-3)	12439-13595	4-13
2 Double Transitions	O_1(J=2-5) + S_2(J=0-4)	11498-12899	0-16
	S_1(J=0-3) + O_2(J=2,3)	11986-12597	0-8
	Q_1(J=0-5) + Q_2(J=0-4)	11988-12248	4-22
	Q_1(J=0-5) + S_2(J=0-5)	12480-13376	4-31
	S_1(J=0-5) + Q_2(J=0-3)	12412-13534	4-22
	S_1(J=0-2) + S_2(J=0-3)	12904-13702	4-13
3 Triple	$Q_1(J_1) + Q_1(J_2) + Q_1(J_3)$	12300-12700	8
4	Overlap transition Q_{3ov}(J=0-5)	11793-11798	2-5

TABLE 2. Assignment of the observed absorption peaks and the dip of the H_2-H_2 second overtone region.

Peak number	Wavenumber of observed peak cm^{-1} at 77K [7,8,19]	Wavenumber of observed peak cm^{-1} at 201 [8]	Wavenumber of observed peak cm^{-1} at 85 [5,6]	Wavenumber of observed peak cm^{-1} at 298 [8,20]	Assignment
1	11773-11775	11732	11765-11782	11740	$Q_3(J)+Q_0(J)$
2	11793-11798	-	-	-	$Q_3(J)$ $_{overlap}$ dip
3	12120	-	12085-12137	-	$S_3(0)+Q_0(J)$, $Q_3(J)+S_0(0)$
4	12226-12227	12255	12230-12369	12255	$S_3(1)+Q_0(J)$, $Q_2(J)+Q_1(J)$
5	12345	-	-	-	$Q_3(J)+S_0(1)$
6	12560-12562	12572	12568-12585	12571	$S_2(0)+Q_1(J)$, $Q_2(J)+S_1(0)$
7	12760-12762	12786	12760-12800	12780	$S_2(1)+Q_1(J)$, $Q_2(J)+S_1(1)$
8	13100-13107	-	-	-	$S_2(1)+S_1(0)$, $S_2(0)+S_1(1)$
9	13310	-	-	-	$S_2(1)+S_1(1)$

The integrated absorption coefficients $\int \alpha(\nu)d\nu$ of the second overtone region are determined by integrating the areas under the experimental profiles. Fig. 7 represents a plot of $(1/\rho^2)\int \alpha(\nu)d\nu$ *versus* density ρ for the experimental profiles at 298, 201 and 77K. The intercept and the slope of the best straight line, which gives the values of the binary and ternary absorption coefficients, respectively, are calculated by a least-square fit of the experimental data. The binary and ternary absorption coefficients obtained by different researchers are given in Table 3.

An example of the profile analyses is shown in Fig. 8. The B-C and L-B lines were used for this purpose. We fit the Birnbaum-Cohen (BC) line shape function to the experimental profiles. The BC function is given by:

$$W_q^{BC}(\Delta\upsilon)=\frac{1}{2\pi^2 c\delta_1}\exp\left(\frac{\delta_1}{\delta_2}\right)\exp\left(\frac{hc\Delta\upsilon}{2kT}\right)\frac{zK_1(z)}{1+\left(\Delta\upsilon/\delta_1\right)} \quad (16)$$

where

$$z=\left[1+\left(\Delta\upsilon\delta_1\right)^2\right]^{1/2}\left[\left(\frac{\delta_1}{\delta_2}\right)^2+\left(\frac{hc\delta_1}{2\pi kT}\right)^2\right]^{1/2} \quad (17)$$

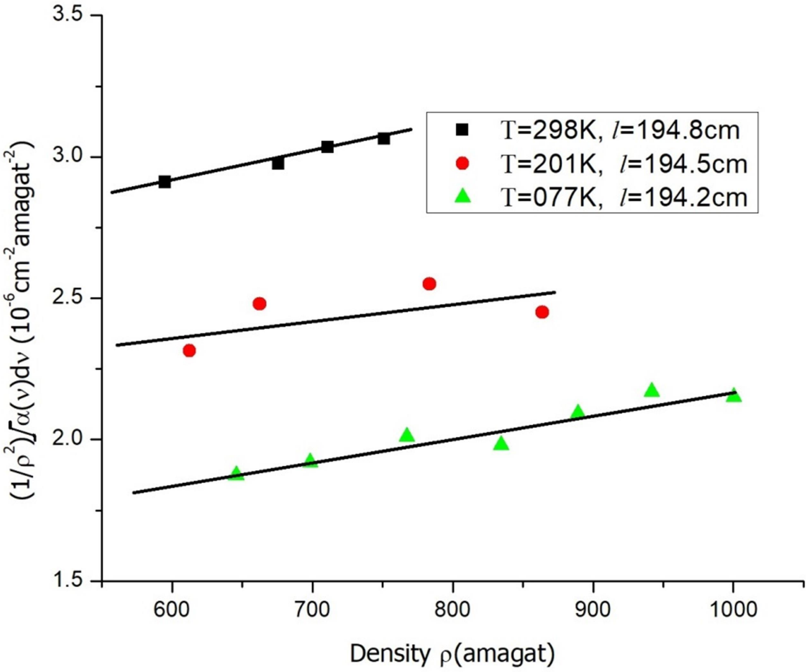

FIG. 7. $(1/\rho^2)\int\alpha(\nu)d\nu$ *versus* density ρ for the experimental profiles at 298, 201 and 77K.

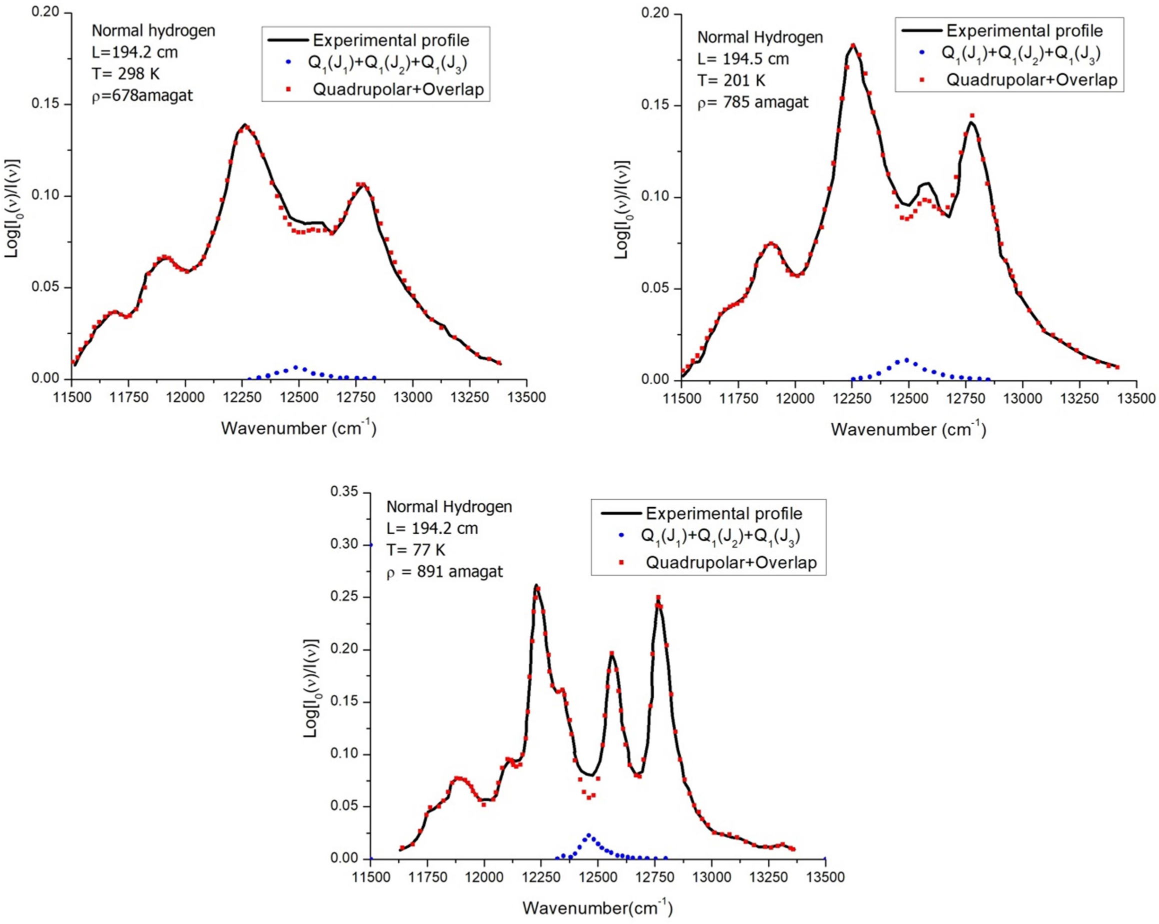

FIG. 8. Analysis of the absorption profile of the second overtone band of H_2-H_2 in the pure gas density 891 amagat at 77 K, density 785 amagat at 201 and density 678 amagat at 298K. The black curve is the experimental profile. The blue square represents the summation of single, double and overlap transitions. The curve represented by red circle around 12,460 cm^{-1} is the difference between the experimental and the previous sum and is attributed to the triple transitions of the type $Q_I(J_1)+Q_I(J_2)+Q_I(J_3)$.

TABLE 3. The binary and ternary absorption coefficients of hydrogen and deuterium (experimental and theoretical values).

Temperature	Binary absorption coefficient $\alpha_1 \times 10^{-6}$ (cm^{-2}amagat^{-2})	Ternary absorption coefficient $\alpha_2 \times 0^{-9}$ (cm^{-2}amagat^{-3})
77K H_2	(1.98±0.20) [19] (1.35±0.04) [8] $\tilde{\alpha}_1=4.53\pm0.3\times10^{-39}$ (cm^{6}s^{-1})] 0.86±0.06[$\tilde{\alpha}_1=4.4\pm0.3$] $\times10^{-39}$ (cm^{6}s^{-1})] [7] [$\tilde{\alpha}_1=7.18$] $\times10^{-39}$ (cm^{6}s^{-1})] [7] (2.10) [11,12] (1.9) [11,12] (calculated)	0.8±0.2 [8] 0.76±0.08 [7]
85K H_2	[$\tilde{\alpha}_1=5.4\times10^{-39}$ (cm^{6}s^{-1})] [5]	
201K H_2	2.13±0.02 $\tilde{\alpha}_1=7.11\times10^{-39}$ (cm^{6}s^{-1})] [8]	0.4±0.1 [8]
298K H_2	(3.25±0.07) [20] (2.33±0.02) $\tilde{\alpha}_1=7.88\times10^{-39}$ (cm^{6}s^{-1})] [8] (3.14) (2.74) [11,12] (calculated)	0.9±0.3 [8]
77K D_2	(0.17±0.05) [$\tilde{\alpha}_1=0.78\pm0.24$] $\times10^{-39}$ (cm^{6}s^{-1})] theory [2.14×10^{-39}] [7]	[$\tilde{\alpha}_1=0.32\pm0.06$] $\times10^{-39}$ (cm^{6}s^{-1})] [7]

It is applied in the case of quadrupolar, single, double and triple transitions. Also, the Levine-Birnbaum (LB) line shape function is applied for the overlap transitions and reads:

$$W_{ov} = \left(\frac{2\Delta\upsilon}{\delta_d}\right)^2 K_2\left(\frac{2\Delta\upsilon}{\delta_d}\right)\left[1-\frac{\gamma}{1+\left(\frac{2\Delta\upsilon}{\delta_c}\right)^2}\right] \tag{18}$$

A typical CIA spectrum of H_2-H_2 in the 3-0 band recorded at a gas density of 891 amagat at 77 K is shown in Fig. 9, where $Log\,[I_0(\nu)/I(\nu)]$ is plotted *versus* the wave-number $\nu(cm^{-1})$. The positions of several transitions are marked a long the wave-number axis. The black curve represents the experimental profile. The dashed curves show the individual quadrupolar components and the red solid line represents the individual overlap components. The green circles represent the sum of the overlap and the quadrupolar components.

A good fit between the experimental and the synthetic profile is obtained except in the range 12300-12700 cm^{-1}. The difference between the recorded and the sum profile is interpreted as arising from the triple transitions $Q_1(J_1) + Q_1(J_2) + Q_1(J_3)$ of hydrogen with (J_1, J_2, J_3) tacking values (111), (110), (100) and (000). These transitions contribute to the absorption, where J takes values 0 and 1 at 77K. Fig. 10 represents absorption profiles of the triple transitions of the type $Q_1(J_1) + Q_1(J_2) + Q_1(J_3)$ of H_2 at 77, 201 and 298 K at different densities of the gas in the second overtone region. The plot of $(1/\rho^3)\int \alpha(\nu)d\nu$ *versus* gas density ρ for the triple transition profiles of H_2 at 77, 201 and 298K is given in Fig. 10. The intercepts obtained from the least-square fit give the ternary absorption coefficients. The calculated values are listed in Table 3.

Profile analyses of the recorded spectrum were carried out using the Birnbaum-Cohen (BC) line shape function for the quadrupolar transitions and the Levine-Birnbaum (LB) line shape function for the overlap transitions. The observed spectra were modeled with synthetic profiles, which are composed of the superposition of an overlap-induced profile and a quadrupolar induced profile. The values of the fitting parameters at different temperatures are given in Table 4.

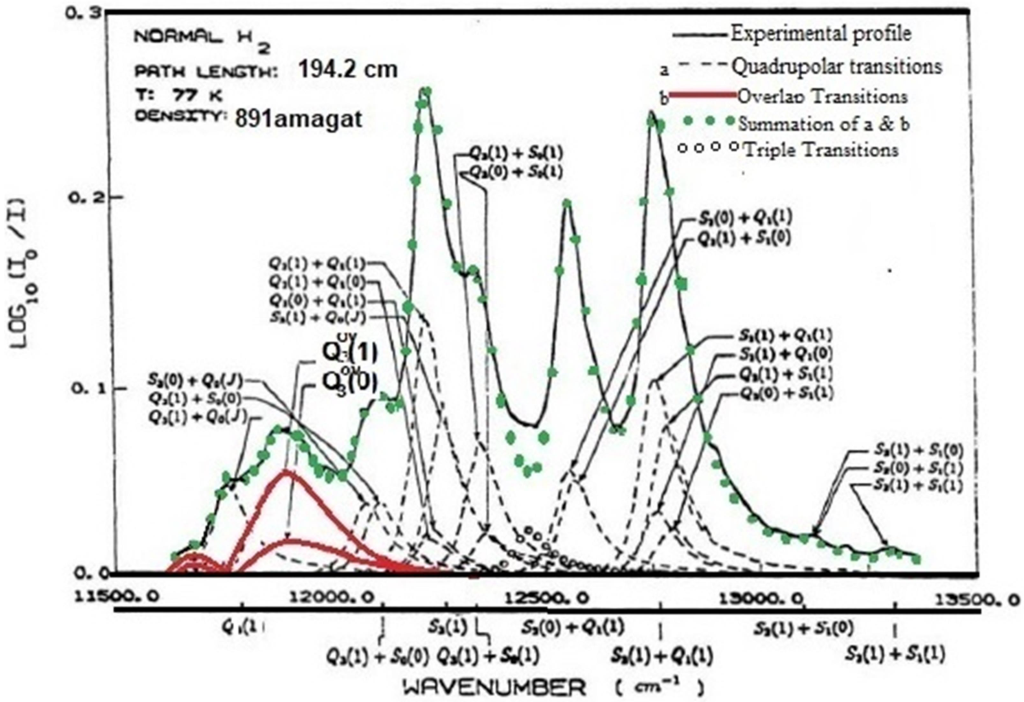

FIG. 9. Analysis of an absorption profile of normal H_2 in the pure gas at 891 amagat and 77 K in the second overtone region. Here, the rotational quantum number J takes the values 0 to 3. The black curve is the experimental profile. The red curve represents the computed overlap-induced profiles, while the dashed curves are quadrupoler-induced profiles. The green circles represent the sum of the computed overlap and quadrupolar components. The difference between the experimental and the sum represented by the curve in open circles is the contribution due to triple transitions.

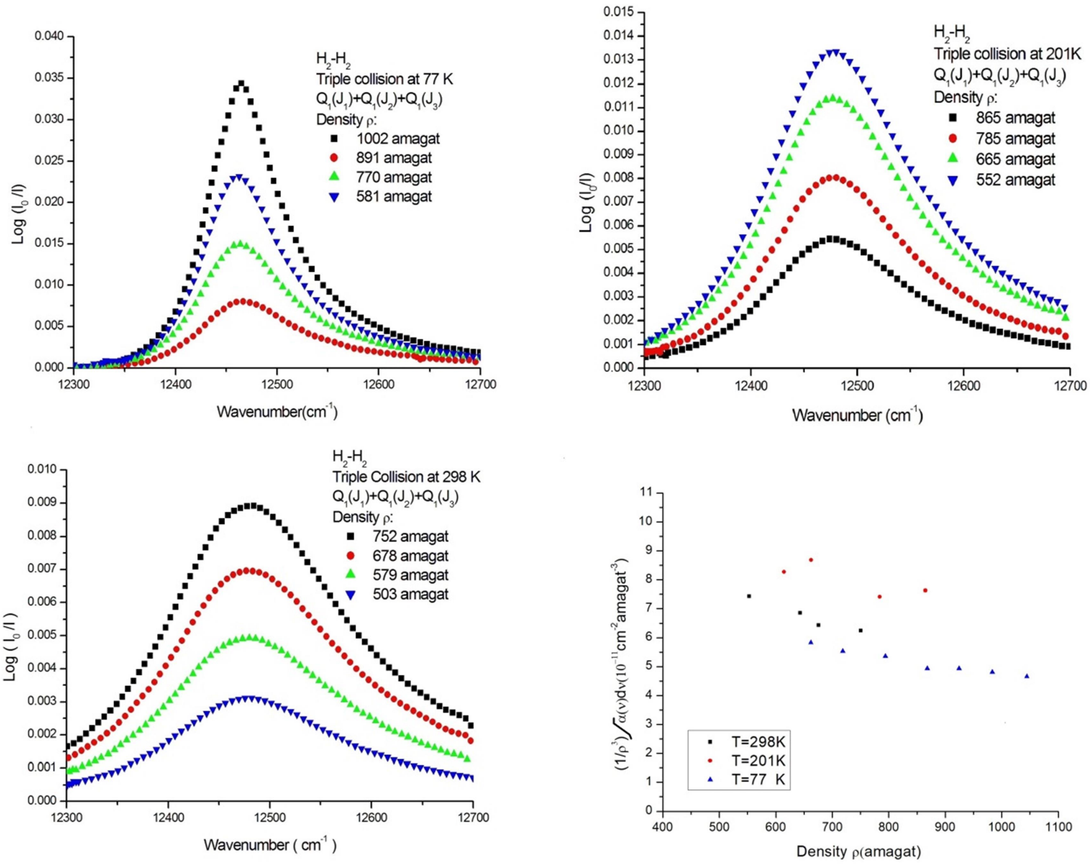

FIG. 10. Absorption profiles of the triple transitions of H_2-H_2-H_2 and $(1/\rho^3)\int\alpha(\nu)d\nu$ *versus* density ρ for the experimental profiles at 298, 201 and 77K.

TABLE 4: Results of profile analysis of H_2-H_2 in the 3-0 band [8, 9].

T	Intra-collisional half-width	Collision duration	Quadrupolar half-width	Collision duration	BC Profile parameters	BC Profile parameters	Overlap contribution	Quadrupolar contribution
(K)	δ_d (cm^{-1})	τ_d (10^{-14}s)	δ_q (cm^{-1})	τ_q(10^{-14}s)	δ_1 (cm^{-1})	δ_2 (cm^{-1})	(%)	(%)
77	98±3	5.4	50±1	11.1	47±3	315±4	11	89
201	104 ±3	5.1	82±1	6.5	100±1	297±3	15	85
298	118±6	4.5	106±3	5.0	135±5	264±4	19	81

Summary of Theoretical Work

A semi-empirical numerical method has been used to compute the binary collision-induced roto-vibrational spectra of hydrogen complexes in the second overtone region at different temperatures. Also, quantum mechanical computation was used to calculate the second overtone profile of hydrogen [11-14].

This code is modified by Borysow and her group. Illustrative examples are given in Fig. 11 and Fig. 12. Fig. 11 shows two profiles calculated at 77 and 298K using the semi-empirical method. Fig. 12 represents two profiles calculated with two methods of normal hydrogen at 77K. These figures are calculated using the code given by Borysow, see:

https://www.astro.ku.dk/~aborysow/programs/.

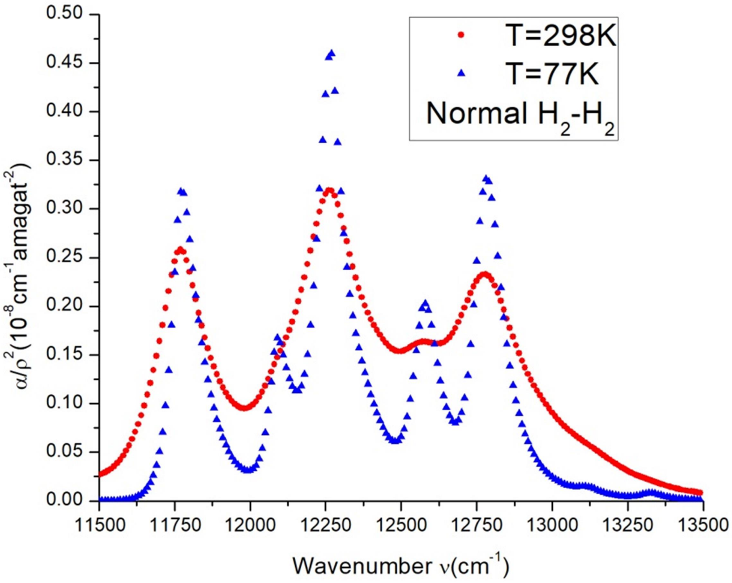

FIG. 11. Two profiles of the CIA spectra calculated theoretically at 77 and 298K.

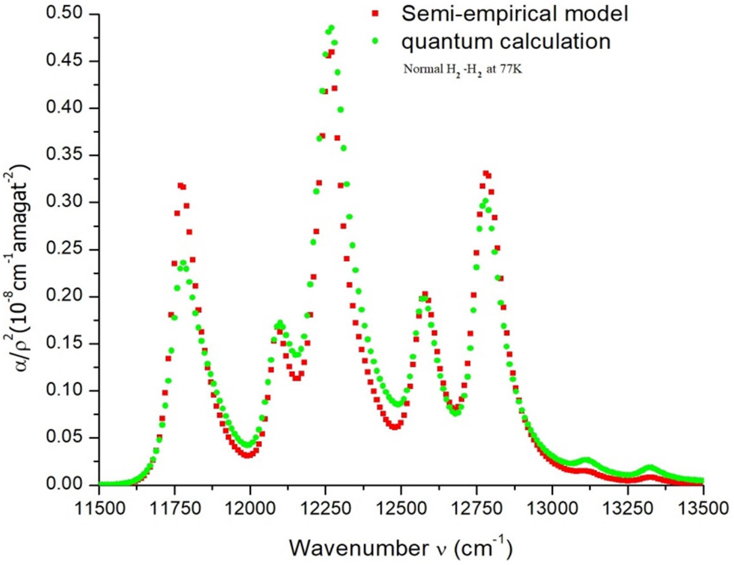

FIG. 12. Theoretical calculations of the CIA spectra of hydrogen at 77K.

Conclusion

The spectra of the second overtone band of H_2-H_2 at 77, 201 and 298K were recorded for different gas densities. Profile analyses of these spectra were carried out using the Birnbaum-Cohen (BC) line shape function for the quadrupolar transitions and the Levine-Birnbaum (LB) line shape function for the overlap transitions. The observed spectra were modeled with synthetic profiles, which are composed of the superposition of an overlap-induced profile and a quadrupolar induced profile. Satisfactory agreement of the measurements with the calculated profiles was observed. The calculated binary and ternary absorption coefficients are in good agreement with theoretical values found by other researchers.

We have reviewed the second overtone band spectra of H_2-H_2 spectra at different temperatures and densities that were studied since 1949. The aim of this article has been to shed more light on the important results obtained since then.

Acknowledgments

The authors are grateful to Asaad R. Sakhel and Basim N. Bulos for their valuable comments on the article.

References

[1] Frommhold, L., “Collision-induced absorption in gases”, (Cambridge University Press, 1993).

[2] Kuiper, G.P., Astrophys. J., 109 (1949) 540.

[3] Herzberg, G., Astrophys. J., 115 (1952) 377.

[4] Hunt, J.L., Ph.D. Thesis, University of Toronto, (1959), Canada.

[5] McKellar, A.R.W. and Welsh, H., Proc. Roy. Soc. Lond. A, 322 (1971) 421.

[6] Welsh, H.L., “Pressure-induced absorption spectra of hydrogen”, Ed. D. Ramsay (Butterworths, London, 1972).

[7] Gillard, P.G., Ph.D. Thesis, Memorial University of Newfoundland, (1983), Canada.

[8] Xiang, F., M.Sc. Thesis, Memorial University of Newfoundland, (1992), Canada.

[9] Reddy, S.P., Xiang, F. and Varghese, G., Phys. Rev. Letters, 74 (1995) 367.

[10] Moraldi, M. and Frommhold, L., Phys. Rev. Letters, 74 (1995) 363.

[11] Brodbeck, C., Bouanich, J., Thanh, N. and Borysow, A., Planetary and Space Science, 47 (1999) 1285.

[12] Brodbeck, C., Bouanich, J., van Thanh, N., Fu, Y. and Borysow, A., J. Chem. Phys., 110 (1999) 4750.

[13] Fu, Y., Zheng, C. and Borysow, A., JQSRT, 67 (2000) 203.

[14] Borysow, A., Borysow, J. and Fu, Y., Icarus, 145 (2000) 601.

[15] Borysow, A., Jorgensen, U.G. and Fu, Y., JQSRT, 68 (2001) 235.

[16] Abel, M., M.Sc. Thesis, The University of Texas, (2009), Austin.

[17] Abel, M., Frommhold, L. and Gustafsson, M., Journal of Chemical Physics, 131 (2009) 181102.

[18] Abu-Kharma, M., Shawagfeh, N. and Gillard, P., 20th ICSLS Ed. J. Lewis, Predio-Cross. AIP (2010) 245.

[19] Abu-Kharma, M., Can. J. Phys., 90 (2012) 339.

[20] Abu-Kharma, M., J. Mol. Spect., 48-50 (2015) 308.

[21] Poll, J.D., Proc. Symposium, I.A.U., No. 40 on Planetary Atmospheres (Morfa, Texas, Dordrecht: Reidel, 1969).

[22] Lewis, J.C., Spectral Line-shapes, Ed. M. Roger Herman, (American Institute of Physics, 1999).

[23] Bragg, S.L. Brault, J.W. and Smith, W.H., Astrophys. J., 263 (1982) 999.

[24] Foltz, J.V., Rank, D.H. and Wiggins, T.A., J. Mol. Spect. 21 (1966) 203.

[25] Rose, M.E., “Elementary Theory of Angular Momentum”, (John Wiley and Sons, Inc. NY, 1957).

[26] van Kranendonk, J., Can. J. Phys., 46 (1968) 1173.